RSC Advances

Journal Name

ARTICLE

Modulating Photogenerated Electron Transfer with Selectively Exposed Co-Mo Facet on a Novel Amorphous g-C$_3$N$_4$/Co$_x$Mo$_{1-x}$S$_2$ Photocatalyst

Xuqiang Hao[a], Zhiliang Jin[a]*, Shixiong Min[a], Gongxuan Lu[b]

A novel photocatalysts g-C$_3$N$_4$/Co$_x$Mo$_{1-x}$S$_2$ with different exposed facets of Co-Mo was employed as catalysts for the examination of facet-dependent catalytic activity toward photocatalytic hydrogen evolution from water splitting with Eosin Y photosensitized as antenna molecule under visible light irradiation. The studies displayed that the g-C$_3$N$_4$/Co$_x$Mo$_{1-x}$S$_2$ photocatalysts had the higher activities than those of g-C$_3$N$_4$/MoS$_2$ and g-C$_3$N$_4$/CoS$_x$. The promoter Co atoms associated with Mo displayed the synergistic effects and efficiently induced photo-generated charge carriers and electron transfer. A possible reaction mechanism of the g-C$_3$N$_4$/Co$_x$Mo$_{1-x}$S was corroborated by photo-luminescence spectra, photo-electro-chemical characterizations and electro-chemical impedance spectrum studies. This study discloses the facet-dependent effect of metal-metal cocatalyst on semiconductor photo-catalysts in photo-catalytic water reduction, and will give an insight into design and synthesis of high-efficient metal/semiconductor hybrid photocatalysts.

Introduction

Hydrogen energy is considered as an ultimate clean fuel in the near future because of its high-energy capacity, environmental benignancy, and recycling utilization. Photocatalytic splitting of water for hydrogen evolution using semiconductor photocatalysts has been regarded as an attractive and promising route to produce hydrogen energy [1]. Currently, various semiconductor photocatalysts have been reported to catalyze the production of hydrogen from water [2-15]. However, most of these catalysts are active only under UV irradiation which take only about 4% of the solar spectrum and photocatalysts for practical use with relatively high productivity under visible light have not yet been found. Thus, searching for simple and efficient photocatalysts utilizing visible light (~ 43% of the solar energy) is of great importance for practical

application.

The recently discovered polymeric graphitic carbon nitride (g-C$_3$N$_4$), has attracted increasing attention as a promising candidate for photocatalytic water splitting due to the appropriate band gap of about 2.7eV [4-6]. The photocatalytic H$_2$ evolution activity of pristine g-C$_3$N$_4$ remains poor because of its low separation efficiency of photogenerated electron-hole pairs [7], and it can be promoted via various chemical modifications, such as doping [8,9], coupling with metals [10], nanostructure engineering [11], organic dyes [12], and hybridization [13,14]. The type and amount of surface co-catalyst are critical factors for efficient utilizing solar energy and enhancing the hydrogen evolution efficiency. However, the co-catalysts used are mainly noble metals such as Pt, which is an excellent co-catalyst for hydrogen production due to its high activity and low overpotential for proton reduction, but it is scarce and expensive for widespread use [14,15]. Therefore, more efforts in searching low-cost co-catalysts based on non-noble metals with better catalytic activities should be devoted. Recently, the MoS$_2$/g-C$_3$N$_4$ composite photocatalysts were prepared via a facile impregnation method and the 0.5wt% MoS$_2$-g-C$_3$N$_4$ sample shown the highest catalytic activity compared to the unmodified g-

RSC Advances Accepted Manuscript

C_3N_4. It was proved that the MoS_2 co-catalysts can efficiently promote the separation of photogenerated charge carriers in g-C_3N_4, and consequently enhance the H_2 evolution activity[16]. Meanwhile, a novel cobalt–phosphate (Co–Pi) modified graphitic carbon nitride (g-C_3N_4) photocatalysts was synthesized by "*in situ*" surface photodeposition process. The Co–Pi catalysts can promote the separation of photogenerated charge carriers in g-C_3N_4 and enhance H_2 and O_2 evolutions too[17]. These serial investigations indicated that these strategies to enhance the photocatalytic H_2 evolution activity are still potential.

The MoS_2 has a highly anisotropic layer structure samples with different edge where the catalytic reaction preferentially occur [18]. The reactions are favored on the edge surfaces of MoS_2 although the active sites may have different degrees of coordinative unsaturation. Coordinatively unsaturated sites along the edges of catalyst particles are believed to provide the active sites, where the molecules can absorb and undergo further reactions [19]. Recently, the layered molybdenum disulfide (MoS_2) has been extensively investigated as a promising catalyst for H_2 generation due to its high activity and low cost [20, 21]. It was reported that the one dimensional MoS_2 nanosheet as cocatalyst loading to porous TiO_2 nanowire exhibit high activity in visible light photocatalytic hydrogen evolution reaction [22]. And others decorated MoS_2 sheets on graphitic C_3N_4 by in situ light-assisted preparation of g-C_3N_4/MoS_2 photocatalysts, which significantly enhanced the H_2 evolution activity due to the MoS_2 can efficiently promote the separation of the photogenerated electrons and holes of g-C_3N_4 [23]. According to these experimental results, it seem that MoS_2 sheets can serve as excellent co-catalyst to composite with semiconductors, and can significantly enhanced the H_2 evolution activity.

Cobalt based compounds (eg: Co_3O_4) showed quite high activity for oxygen and hydrogen generation due to its low overpotential and convenient redox transformation between different chemical valence states (eg: Co^{2+}, Co^{3+}) [24-27]. It was reported that Co_3O_4 nanocrystals grown on reduced graphene oxide as a high-performance bi-functional catalyst for the oxygen reduction reaction and oxygen evolution reaction[28]. Alberto et al. have synthesized F-doped Co_3O_4 films, which exhibited high hydrogen generation activity with respect to the corresponding undoped oxide [29]. Pu et al. have reported CoP nanosheet arrays supported on a Ti plate as an efficient cathode for electrochemical hydrogen evolution[30]. These results were proposed Co as potential candidates for replacing noble metal catalysts.

The commonly used hydrotreating catalysts of Co

atoms as a promoter added in MoS_2 formation of so-called Co-Mo-S structures. The catalytically most interesting Co-Mo-S structures phase has an MoS_2-like texture, which lead to an increased reactivity compared to pure Mo edge sites. It was observed that the key of identification of the Co-Mo-S structures could be responsible to the promotion of the catalytic activity [31-33]. It has been suggested that the Co-promoter is to facilitate forming corrdinatively unsaturated metal sites by reducing the sulfur binding energy at the edge [19].

Herein, we described a high efficient non-noble metal cobalt co-catalyst implanted on the MoS_2 sheets decorated g-C_3N_4 (g-C_3N_4/$Co_xMo_{1-x}S_2$) for hydrogen production. After sensitization by Eosin Y, this noble-mental-free photocatalyst with different exposed facets of Co-Mo exhibited high photocatalytic hydrogen evolution activity under visible light irradiation. The excellent photocatalytic activity might be ascribed to the synergistic effect of g-C_3N_4/MoS_2 and Co-Mo-S structure. In addition, the corresponding fluorescence results indicated that the charge separation efficiency and photogenerated electrons transfer from excited dye to the hydrogen evolution active sites was remarkably promoted, and consequently enhanced the photocatalytic activity for hydrogen evolution. The effects of g-C_3N_4 content on the photocatalytic hydrogen evolution activity were investigated. This report may provide new method for preparation of high-active and low-cost catalyst for hydrogen evolution.

Experimental

Preparation of g-C_3N_4/$Co_xMo_{1-x}S_2$ composite photocatalysts

All chemicals were reagent grade and used without further purification. The mental-free g-C_3N_4 powder was synthesized by directly heating melamine in a muffle furnace. In a typical synthesis, 5g melamine was heated at 550 °C for 4 h in a semiclosed system with a cover. After the furnace was allowed to cool to room temperature, the resultant yellow products was collected and ground into a powder for further use.

The g-C_3N_4/$Co_xMo_{1-x}S_2$ composite photocatalysts were synthesized using a facile solvothermal method. Typically, the as-prepared 125mg g-C_3N_4 sample was first dispersed in deionized water (40mL) with the ultrasound treatment at room temperature until the solution becomes a homogeneous dispersion. Then, 1.25g $(NH_4)_6Mo_7O_{24}\cdot4H_2O$ and 0.125g $Co(NO_3)_2\cdot6H_2O$ was added to the g-C_3N_4 dispersed solution under magnetic stirring. After it dissolved, 25mL of aqueous solution containing 3.2g $Na_2S\cdot9H_2O$ was added to the mixture slowly. The

mixture was then stirred at room temperature for 30 min, the as-formed homogeneous solution was then transferred into a 100 mL Teflon-lined stainless steel autoclave, maintained at 160 °C for 10h. Subsequently, the autoclave was cooled to room temperature gradually. The product was filtrated and washed several times with distilled water and ethanol, dried at 40 °C for 5 h. Pure g-C_3N_4/CoS_2 and g-C_3N_4/MoS_2 were fabricated through a similar procedure. According to this method, g-C_3N_4/$Co_xMo_{1-x}S_2$ composites with different g-C_3N_4 mass ratios from 10 to 50% were synthesized.

Characterization

The X-ray diffraction (XRD) patterns of the samples were recorded on a Rigaku B/Max-RB diffractometer with a nickel filtrated Cu Kα radiation operated at 40 kV and 30 mA. Filed emission scanning electron microscopy (FESEM) images were recorded on a JSM-6701F scanning electron mircroscope operated at an accelerating voltage of 5.0 kV. Transmission electron microscopy (TEM) and high-resolution TEM(HRTEM) images were taken with a Tecnai-G2-F30 field emission transmission electron microscope operating at an accelerating voltage of 300 kV. X-ray photoelectron spectroscopy (XPS) measurements were performed on K-Alpha-surface Analysis(Thermon Scientific) using X-ray monochromatization. Photoluminescence data (PL) were acquired using a FLUOROMAX-4 spectrophotometer at room temperature.

Photocatalytic H$_2$ evolution experiments

Photocatalytic experiments were conducted in a one-compartment Pyrex cell ca.162 cm^3 having a flat window ca.10.2 cm^2 for illumination. In a typical photocatalytic experiment, 20mg of catalyst was suspended in 100 ml 10% (v/v) triethanolamine (TEOA) aqueous solution contain 28mg dye Eosin Y (EY) by means of a magnetic stirrer. The opening of the cell was sealed with a silicone rubber septum. The reactant mixture was degassed by bubbling N$_2$ gas for 40 min, and then was irradiated by a 300-W Xe lamp with a cutoff filter of 420 nm for H$_2$ evolution under magnetic stirring condition and measurements of the photocatalytic H$_2$ evolution activity. The amount of hydrogen evolution was measured using gas chromatography (Tianmei GC7900, TCD, 13Xcolumn, N$_2$ as carrier).

The stability testing of H$_2$ evolution over EY-g-C_3N_4/$Co_{0.04}Mo_{0.96}S_2$-30% was conducted every 14h for 4 times. The pH of TEOA solution was adjusted by concentrated hydrochloric acid (HCl).

All glassware was rigorously cleaned and carefully rinsed with distilled water prior to use.

Photoelectrochemical measurements

The photoelectrochemical measurement was performed on an electrochemical analyzer (PAR VersaSTAT 4) in a homemade standard three-electrode cell[3]. Platinum foil was used as the counter electrode, and a saturated calomel electrode (SCE) as the reference electrode. The working electrodes were prepared by drop-coating homogeneous catalyst suspensions directly onto the precleaned indium tin oxide glass (ITO glass) surface, and then 500 μL of EY aqueous solution (4.0×10^{-4} mol/L) was added onto the above catalyst film electrode surface and then dried. The supporting electrolyte was 10v/v% TEOA (pH 9) mixed with 0.1 mol/L Na$_2$SO$_4$ aqueous solution. The surface area of the working electrode exposed to the electrolyte was about 0.95 cm^2. A 300-W Xe lamp equipped with an optical cutoff filter of 420 nm was used for excitation.

Results and discussion

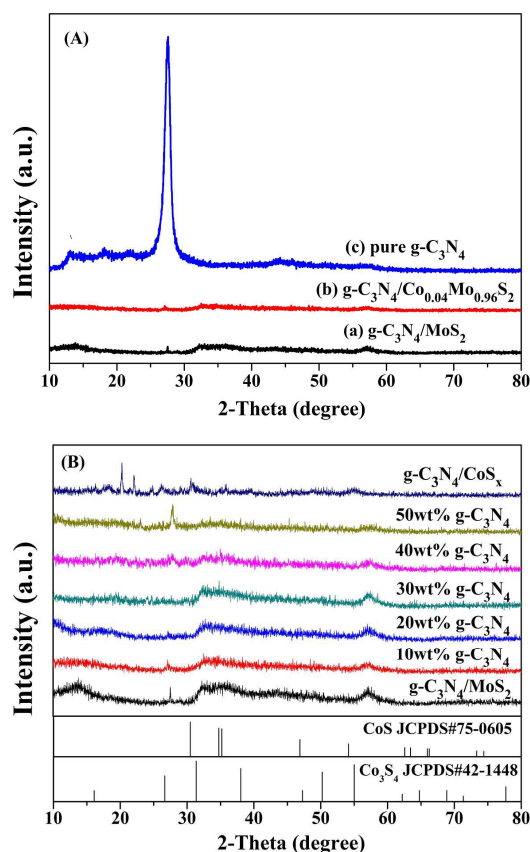### XRD analysis

Fig.1 (A) X-ray diffraction (XRD) patterns of g-C_3N_4/MoS_2, g-C_3N_4/$Co_{0.04}Mo_{0.96}S_2$ and pure g-C_3N_4; (B) XRD patterns of g-C_3N_4/MoS_2, g-C_3N_4/CoS_x and the g-C_3N_4/$Co_{0.04}Mo_{0.96}S_2$

composites with different g-C_3N_4 mass ratios from 10 to 50%.

To certify the successful fabrication of the g-C_3N_4/$Co_{0.04}Mo_{0.96}S_2$ nanocomposite, the as-prepared sample was investigated by powder X-ray diffraction (XRD). In Fig.1-A, The XRD peak of pure g-C_3N_4 sample is in good agreement with the hexagonal phase of g-C_3N_4 (JCPDS#87-1526). The pure g-C_3N_4 sample shows two distinct peaks at 27.4° (d = 0.336 nm) and 13.1° (d = 0.765nm). The former peak is attribute to the (002) plane with graphitic stacking, the letter weak diffraction peak is related to the (100) in-plane structural repeating units of tri-s-triazine. These two diffraction peaks are good agreement with the g-C_3N_4 reported in the literature [34]. When the MoS_2 loading, the g-C_3N_4/MoS_2 has four discernible diffraction peaks, which confirms the three typical peaks at 14.1°, 33.7° and 58.7° belong to (002), (101) and (110) planes of hexagonal MoS_2 (JCPDS#75-1539), respectively. The XRD pattern of g-C_3N_4/CoS_x showed in Fig. 1-B, the CoS_x was a mixture of cubic Co_3S_4 (JCPDS#42-1448) and hexagonal CoS (JCPDS#75-0605). The diffraction peaks at 26.6°, 31.3° and 55.0° were determined as the (220), (311) and (440) diffraction signals of Co_3S_4, while the two peaks located at 30.6° and 47.1° belonged to (100) and (102) planes of hexagonal CoS. There is no obvious difference can be observed in g-C_3N_4/$Co_{0.04}Mo_{0.96}S_2$ nanocomposite with g-C_3N_4/MoS_2 when the Co doped, except for a gradually decrease in the diffraction intensity as the g-C_3N_4 content increased. This result indicates an inhibition of composite condensation by excessive g-C_3N_4. Besides, there is not any peak belonged to cobalt or other cobalt species. These results strong indication that cobalt was incorporated in the g-C_3N_4/MoS_2 framework and the well-dispersed Co-Mo-S nanoclusters on the sheets of g-C_3N_4 substrate formed amorphous g-C_3N_4/$Co_{0.04}Mo_{0.96}S_2$ nanocomposite.
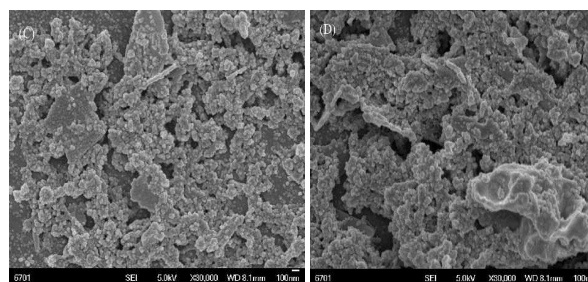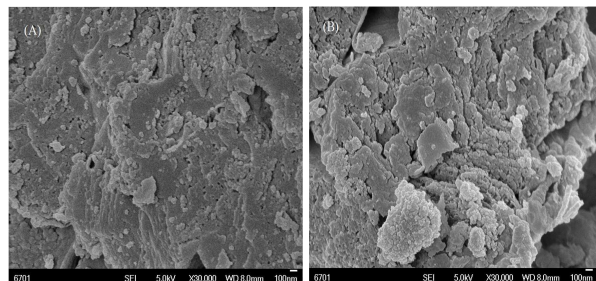
SEM characterization

Fig.2 SEM images of the as-prepared samples: (A)-(B) Pure g-C_3N_4; (C)-(D) g-C_3N_4/$Co_{0.04}Mo_{0.96}S_2$ photocatalysts.

The morphologies of g-C_3N_4/$Co_{0.04}Mo_{0.96}S_2$ composite photocatalyst was analyzed by SEM. Fig.2 presents the SEM images of pure g-C_3N_4 and g-C_3N_4/$Co_{0.04}Mo_{0.96}S_2$ composite samples. The pure g-C_3N_4 sheets are prone to multi-stack mesoporous structures with nanocovalent π-π and much hollows can be observed on the surface（Fig.2 A-B）. The $Co_{0.04}Mo_{0.96}S_2$ co-catalysts (in Fig.2 C-D) are presented as irregular nanoparticles on the g-C_3N_4 sheets in the composite samples, and it appears to have aggregated microstructures comprising a number of 50 – 200 nm irregular particles.
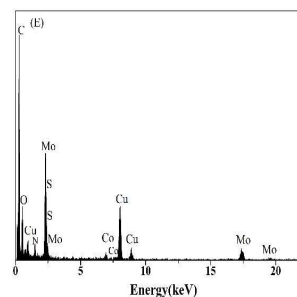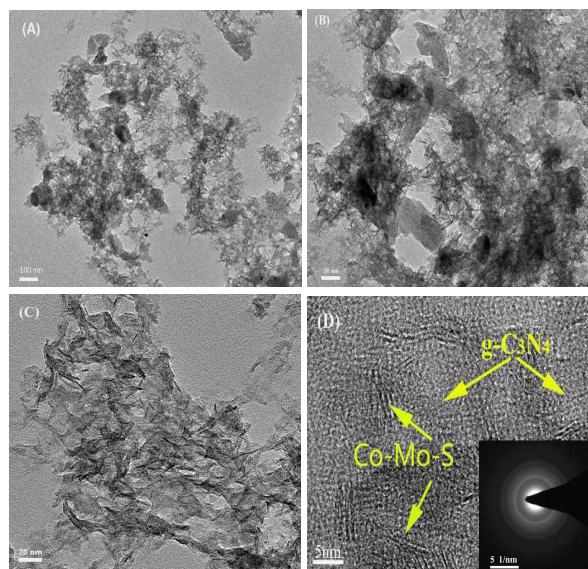
TEM characterization

Fig.3 A-B and C-D are the TEM and HRTEM images for g-C_3N_4/$Co_{0.04}Mo_{0.96}S_2$ nanohybrid. The inset in D is the corresponding SAED pattern. (E) EDS spectrum of g-C_3N_4/$Co_{0.04}Mo_{0.96}S_2$ in which the Cu signals originated from the Cu grid support for TEM observation.

The transmission electron microscopy (TEM) images of g-C_3N_4/$Co_{0.04}Mo_{0.96}S_2$ nanohybrid (Fig.3-A,B) revealed that large amounts of the amorphous component adhered on the surface of g-C_3N_4 sheets. The high-resolution TEM (HRTEM) image in Fig.3-C clearly indicate that the g-C_3N_4/$Co_{0.04}Mo_{0.96}S_2$ catalyst contain the Co in the form of MoS_2-like Co-Mo-S structures, the $Co_{0.04}Mo_{0.96}S_2$ sheets are prone to stacking together with the g-C_3N_4 sheets and formation of multi-stack structures. In Fig.3-D, the lattice fringes are not clear enough to confirm the d values and the facets via the lattice fringes, which testified the g-C_3N_4/$Co_{0.04}Mo_{0.96}S_2$ was an amorphous materials. The selected area electron diffraction (SAED) pattern of g-C_3N_4/$Co_{0.04}Mo_{0.96}S_2$ (inset in Fig. 3-D) further confirmed the amorphous nature of the particles. The energy dispersive X-ray (EDS) results confirmed the co-existence of C, N, Co, Mo and S elements in the line and area of lattice fringes of g-C_3N_4/$Co_{0.04}Mo_{0.96}S_2$ nanohybrid (Fig.3-E), which was supported by the XRD pattern of g-C_3N_4/$Co_{0.04}Mo_{0.96}S_2$.

X-ray photoelectron spectroscopy (XPS)
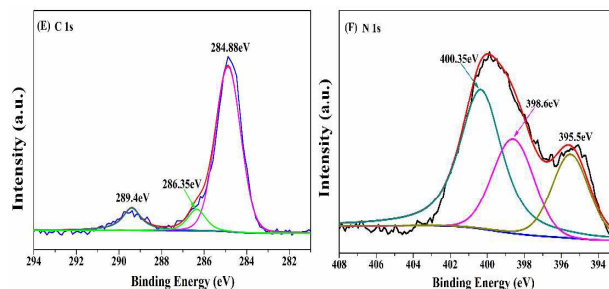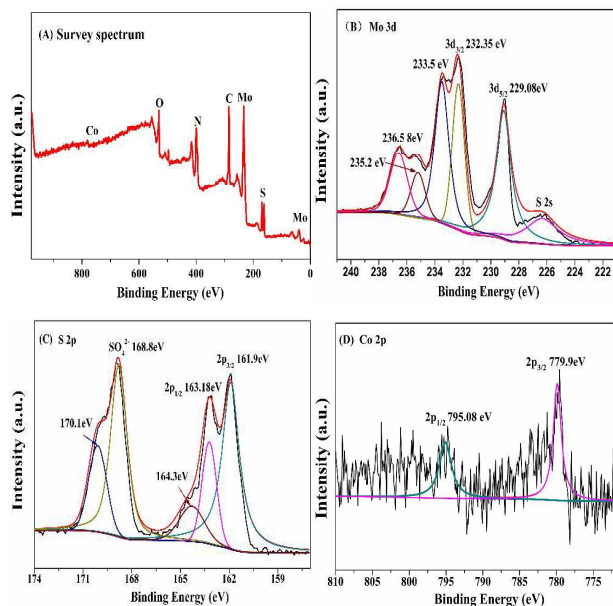
Fig.4 (A) XPS survey spectra of g-C_3N_4/$Co_{0.04}Mo_{0.96}S_2$ sample, (B) Mo 3d, (C) S 2p, (D) Co 2p, (E) C1s and (F) N 1s scan spectra of g-C_3N_4/$Co_{0.04}Mo_{0.96}S_2$ sample.

The g-C_3N_4/$Co_{0.04}Mo_{0.96}S_2$ sample was further characterized by X-ray photoelectron spectroscopy (XPS), revealing that the catalyst mainly consist of Mo, S, O, Co, C and N elements (Fig.4-A). The binding energies of Mo $3d_{3/2}$ (232.35 eV) and Mo $3d_{5/2}$ (229.08 eV) in Fig.4-B indicated Mo as Mo^{4+} in the g-C_3N_4/$Co_{0.04}Mo_{0.96}S_2$ sample [35]. In Fig.4-C, the peak at 161.88 eV was ascribed to S $2p_{3/2}$, while the peak at 163.18 eV could be assigned to S $2p_{1/2}$. And the other peak around 168.8 eV could be attributed to SO_4^{2-} or SO_3^{2-} species, which maybe originate from the sodium sulfide used during synthesis. The Co 2p XPS spectra in Fig.4-D show that the binding energies of Co $2p_{3/2}$ and Co $2p_{1/2}$ for g-C_3N_4/$Co_{0.04}Mo_{0.96}S_2$ occur at 779.9 and 795.08 eV, respectively, which are indicative of Co as Co^{2+} in the g-C_3N_4/$Co_{0.04}Mo_{0.96}S_2$ nanohybrid [22]. In Fig.4-E, two single peaks at 284.88 and 289.4 eV can be observed for C 1s. The former peak is a standard carbon specialized for the catalyst, whereas the latter peak is assigned to carbon atoms bonded with three N atoms in the g-C_3N_4 lattice [9]. In Fig.4-F, the N 1s can be deconvoluted into three peaks at 395.5, 398.6 and 400.35 eV, which represent for nitrogen atoms in the C=N—C, N—$(C)_3$ and C—N—H functional groups in polymeric g-C_3N_4 structures [16]. These results indicate the $Co_{0.04}Mo_{0.96}S_2$ co-catalysts have been successfully introduced into the g-C_3N_4 photocatalyst. According to XPS results, the approximate composition is determined to be g-C_3N_4/$Co_{0.04}Mo_{0.96}S_2$.

Photocatalytic activities over Eosin Y-sensitized g-C_3N_4/$Co_{0.04}Mo_{0.96}S_2$ for H_2 evolution and Stability
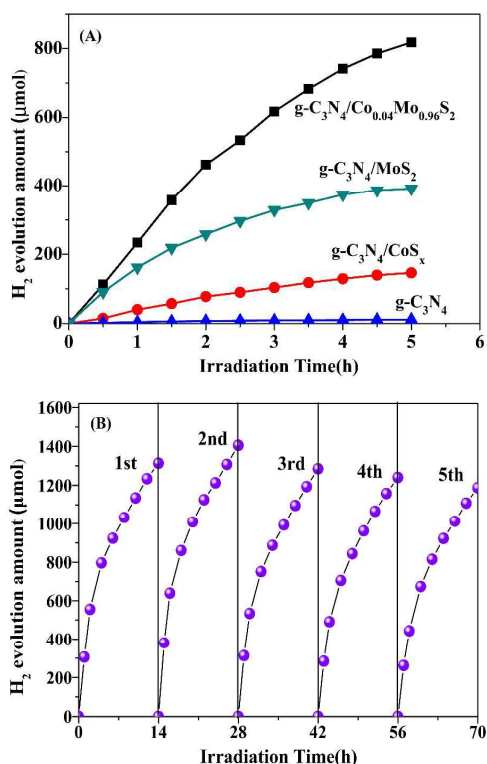
Fig.5 (A) The photocatalytic activities of EY-sensitized $(4.0 \times 10^{-4} M)$ photocatalysts (20mg) for hydrogen evolution (Reaction time: 5h). (B) Stability testing of H_2 evolution over EY-g-C_3N_4/$Co_{0.04}Mo_{0.96}S_2$-30%.

Fig.5-A shows the photocatalytic activities of EY-sensitized g-C_3N_4, g-C_3N_4/CoS_x, g-C_3N_4/MoS_2 and g-C_3N_4/$Co_{0.04}Mo_{0.96}S_2$ nanocomposites in 100mL of 10% (v/v) TEOA aqueous solution under visible light irradiation ($\lambda \geq 420$ nm) at pH 9. As shown in Fig.5-A, the presence of g-C_3N_4 and Co or CoS_x were crucial for improving the photocatalytic H_2 evolution activity. The g-C_3N_4 photocatalyst only 11.24 µmol of H_2 produced after 5h irradiation, suggesting that the g-C_3N_4 itself was inactive for H_2 evolution probably due to its low separation efficiency of photogenerated electron-hole pairs which unfavorable hydrogenated surfaces for H_2 evolution [21]. The amount of H_2 production were 391.85 µmol and 146.59 µmol over the EY-sensitized g-C_3N_4/MoS_2 and g-C_3N_4/CoS_x photocatalyst in 5h, Which significantly enhanced the photocatalytic activity of g-C_3N_4 under the same reaction conditions. When the cobalt incorporated, the photocatalytic activities of g-C_3N_4/$Co_{0.04}Mo_{0.96}S_2$ remarkably enhanced for H_2 production and the maximum amount of H_2 production up to 818.6 µmol, which was 2.25 times than the g-C_3N_4/MoS_2 and 72.8 times than that of same weight of pure g-C_3N_4 under the same reaction conditions. These results indicated that cobalt is a key factor to improve H_2 evolution activity of g-

C_3N_4/MoS_2, and revealed the presence of Co-Mo-S structures in g-C_3N_4/$Co_{0.04}Mo_{0.96}S_2$ nanocomposites which are responsible for the promotion of the reactivity [19]. The Co-promoter atoms occupy sites at edges of so-called Co-Mo-S formation of different exposed facets of Co-Mo, which lead to an increased reactivity compared to pure Mo edge sites. It was suggested that Co promoter is facilitate forming corrdinatively unsaturated metal sites by reducing the sulfur binding energy at the edge in which electron transfer easily can occur from dye to catalyst, thus achieving a high photocatalytic activity.

Furthermore, the stability test of g-C_3N_4/$Co_{0.04}Mo_{0.96}S_2$-30% was carried out. As shown in Fig.5-B, displays the H_2 evolution curve in cycling photocatalytic runs and the g-C_3N_4/$Co_{0.04}Mo_{0.96}S_2$ exhibits high stability. This result showed that EY-sensitized g-C_3N_4/$Co_{0.04}Mo_{0.96}S_2$-30% exhibits high stability during the photocatalytic H_2 evolution processes due to its synergetic effect of g-C_3N_4/MoS_2 interface and the Co-Mo-S structures.

Effect of pH and the g-C_3N_4 (%) on the photocatalytic activity of g-C_3N_4/$Co_{0.04}Mo_{0.96}S_2$

The pH of the solution had a significant influence on the photocatalytic activity. As shown in Fig.6-A, acidic and strongly alkaline conditions are not conducive to hydrogen evolution. The high photocatalytic hydrogen production activity was exhibited at pH 9, and the larger amounts of H_2 evolution was observed in a broader pH range(7-10). The likely reason was that the state of TEOA was effected by pH of the solution, namely, the amount of $^3(EY^{2-})^*$ can be reductively quenched by TEOA absolutely at pH 9 and the dye can be effectively absorbed on the different exposed facets of Co-Mo at this pH.

Furthermore, the influence of weight ratio of g-C_3N_4 to $Co_{0.04}Mo_{0.96}S_2$ in g-C_3N_4/$Co_{0.04}Mo_{0.96}S_2$ on H_2 evolution activity was investigated and a significant impact of g-C_3N_4 content was found. Fig.6-B emphasizes that the g-C_3N_4 content is pivotal for optimal photocatalytic activity: the photocatalytic H_2 evolution increased with the g-C_3N_4 content raise, and it reached a maximum when the weight ratio of g-C_3N_4 to $Co_{0.04}Mo_{0.96}S_2$ was about 30 wt%. When it beyond 30 wt%, a decrease in the photocatalytic H_2 evolution results. The origin of this effect can be explained as follows: the suitable g-C_3N_4 content causes $Co_{0.04}Mo_{0.96}S_2$ has more exposed facets of Co-Mo, which favors the transfer and separation of the charge carriers. At a higher g-C_3N_4 content, the g-C_3N_4 nanosheets would be bulked, reducing the density of g-C_3N_4 active sites and the exposed facets of Co-Mo available for H_2 production. Moreover, a higher g-C_3N_4 content is not in favor of the

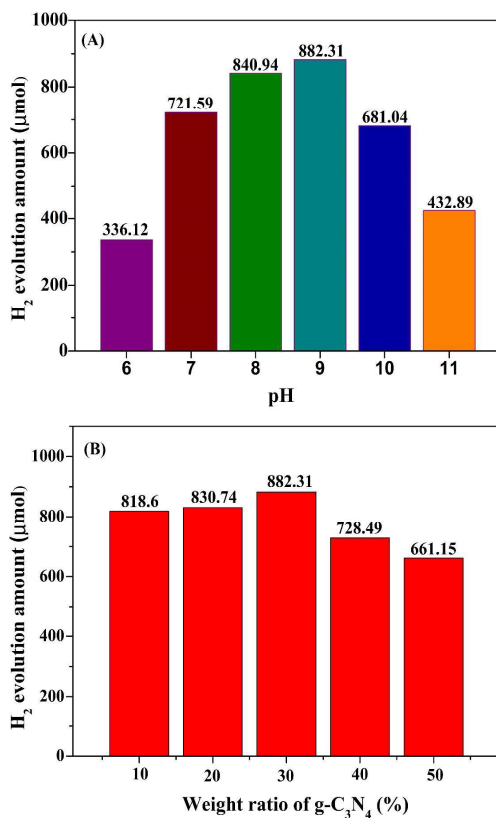separation of electron-hole pairs and the migration of photogenerated electrons.

Fig.6 (A) Effect of the pH on photocatalytic activity of g-C_3N_4/$Co_{0.04}Mo_{0.96}S_2$ (20mg) for hydrogen evolution (Reaction time: 5h); (B) Effect of the different g-C_3N_4 mass ratios from 10 to 50% on photocatalytic activity of g-C_3N_4/$Co_{0.04}Mo_{0.96}S_2$ in 10 % (v/v) TEOA aqueous solution (pH 9) under visible light irradiation.

Photoluminescence (PL) analysis

In order to prove the important role of cobalt in facilitating the transfer of photogenerated electrons to improve the g-C_3N_4/$Co_{0.04}Mo_{0.96}S_2$ nanocomposite photocatalytic activity, the photoluminescence quenching of EY in the presence of g-C_3N_4, g-C_3N_4/CoS_x, g-C_3N_4/MoS_2 and g-C_3N_4/$Co_{0.04}Mo_{0.96}S_2$ were further examined. As shown in Fig.7, EY solution (1×10^{-6} mol/L) excited at 480 nm shows a typically extensive emission peak at 538nm. With the pure g-C_3N_4 was added, a slightly decline occurred. As g-C_3N_4/CoS_x and g-C_3N_4/MoS_2 were introduced into the EY aqueous solution, a significant decrease was observed at an emission wavelength of 538nm, which can be attributed to the two types of semiconductor materials closely combined and the heterojunction structure, the formation of intimate interfaces is believed to promote the migration of photo-

generated electrons to conduction band of catalysts. Thus, the recombination of electron-hole pairs was inhibited, and charge separation as well as stabilization was achieved. Once the cobalt was added, the photoluminescence drops markedly, which indicating that the recombination of photoinduced electron-hole pairs was inhibited greatly due to superior electron acceptor of Co-Mo-S structures, electrical conductivity of g-C_3N_4 and highly hybridized nanostructure, thus accounting for the significantly enhanced hydrogen evolution activity under visible light irradiation.
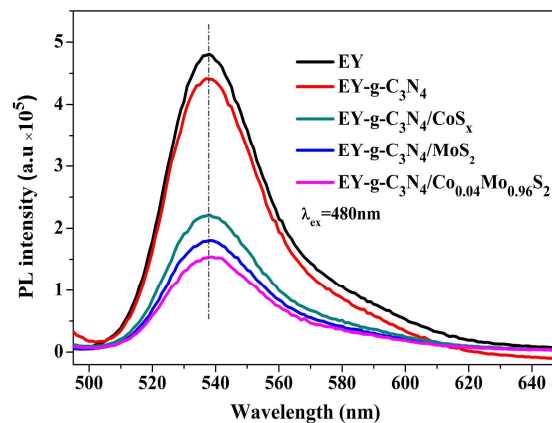

Fig.7 Fluorescence spectra of EY-sensitized g-C_3N_4, g-C_3N_4/CoS_x, g-C_3N_4/MoS_2 and g-C_3N_4/$Co_{0.04}Mo_{0.96}S_2$ samples in 10% (v/v) TEOA aqueous solution at pH 9.

Moreover, the fluorescence lifetime of EY was investigated to further probe the excited charge transfer and confirmed the quenching mechanism. As shown in Table 1, the emission of singlet excited EY follows one-exponential decay with a lifetime of 0.320 ns, which almost kept constant (0.334 ns) in the presence of g-C_3N_4, indicating that the static quenching mechanism governs the quenching of the EY singlet state. The decay of singlet excited state EY was enhanced with the addition of the g-C_3N_4/CoS_x, g-C_3N_4/MoS_2 and g-C_3N_4/$Co_{0.04}Mo_{0.96}S_2$, and the fluorescence lifetimes of long decay components were 3.60, 3.76 and 3.85 ns, respectively. And it can be fitted with two exponential decay functions, which means the presence of dynamic quenching [33]. These results indicated that the lifetime of the singlet excited EY^{1*} could be prolonged in the g-C_3N_4/CoS_x, g-C_3N_4/MoS_2 and g-C_3N_4/$Co_{0.04}Mo_{0.96}S_2$ systems, especially the formation of Co-Mo-S structures with different exposed facets of Co-Mo, which could greatly facilitate the intersystem crossing (ISC) to produce the low-lying triplet excited state (EY^{3*}), then formation of EY$^{•-}$ in the presence of TEOA.

Table 1 Decay parameters of EY in the presence of g-C$_3$N$_4$, g-C$_3$N$_4$/CoS$_x$, g-C$_3$N$_4$/MoS$_2$ and g-C$_3$N$_4$/Co$_{0.04}$Mo$_{0.96}$S$_2$ in 10 % (v/v) TEOA aqueous solution at pH 9.

Systems [a]	Lifetime, $<\tau>$ (ns)	Pre-exponential factors A/%	Average lifetime, $<\tau>$ (ns) [d]	χ^2
EY [b]	τ=0.320	A = 50	0.320	1.002
EY-g-C$_3$N$_4$ [c]	τ_1=0.334	A_1 = 50	0.334	1.003
EY-g-C$_3$N$_4$/CoS$_x$ [c]	τ_1=0.361	A_1 = 97.76	0.360	1.001
	τ_2=3.60	A_2 = 2.24		
EY-g-C$_3$N$_4$/MoS$_2$ [c]	τ_1=0.377	A_1 = 98.12	0.380	0.999
	τ_2=3.76	A_2 =1.88		
EY-g-C$_3$N$_4$ -Co$_{0.04}$Mo$_{0.96}$S$_2$ [c]	τ_1=0.391	A_1 = 97.7	0.493	1.001
	τ_2=3.85	A_2 =2.3		

[a] Decay of TEOA aqueous solution (10% v/v) of 1.0×10^{-6} mol/L EY at pH 9 was recorded in the presence of 0.15 mg/mL g-C$_3$N$_4$, g-C$_3$N$_4$/CoS$_x$, g-C$_3$N$_4$/MoS$_2$ and g-C$_3$N$_4$/Co$_{0.04}$Mo$_{0.96}$S$_2$. The excited and emission wavelength were 480 nm and 538 nm, respectively. [b]Single-exponential fit for EY. [c] Double-exponential fit for EY-g-C$_3$N$_4$, EY-g-C$_3$N$_4$/CoS$_x$, EY-g-C$_3$N$_4$/CoS$_x$ and EY-g-C$_3$N$_4$/Co$_{0.04}$Mo$_{0.96}$S$_2$. [d]Average lifetime $<\tau>$ was determined according to reported method [36].

Photocurrent–time and linear sweep voltammetry (LSV) test

To provide addition evidence for the photocatalytic electron transfer mechanism, the transient photocurrent responses of dye sensitized g-C$_3$N$_4$, g-C$_3$N$_4$/CoS$_x$, g-C$_3$N$_4$/MoS$_2$ and g-C$_3$N$_4$/Co$_{0.04}$Mo$_{0.96}$S$_2$ coated on ITO were investigated for several on-off cycles of intermittent irradiation [3]. As shown in Fig. 8 A, the EY-g-C$_3$N$_4$/Co$_{0.04}$Mo$_{0.96}$S$_2$ composite photocatalyst shows the highest photocurrent intensity of the four samples, whereas the lowest photocurrent intensity can be observed on the EY-g-C$_3$N$_4$ sample. This result additionally reveal the fast interfacial electron transfer from EY$^-$• to g-C$_3$N$_4$/Co$_{0.04}$Mo$_{0.96}$S$_2$ then to g-C$_3$N$_4$, g-C$_3$N$_4$/CoS$_x$ and g-C$_3$N$_4$/MoS$_2$ electrodes, while the excited state dye species will be reductively quenched by the TEOA in the solution to induce an oxidation reaction at the photoelectrode surface [4]. That is, the different exposed facets of Co-Mo could accelerate the charge transfer and lower the charge recombination in the g-C$_3$N$_4$/Co$_{0.04}$Mo$_{0.96}$S$_2$ photocatalytic system. As a result, the photocatalytic H$_2$ evolution activity was enhanced.
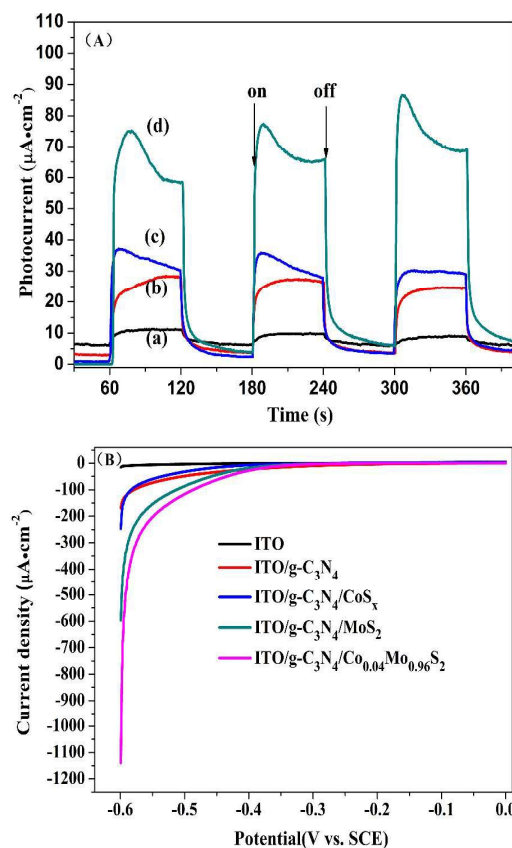

Fig.8 (A) Transient photocurrent response for the EY-sensitized (a) g-C$_3$N$_4$, (b) g-C$_3$N$_4$/CoS$_x$, (c) g-C$_3$N$_4$/MoS$_2$ and (d) g-C$_3$N$_4$/Co$_{0.04}$Mo$_{0.96}$S$_2$ samples. (B) LSV curves of bare ITO glass and EY-sensitized g-C$_3$N$_4$, g-C$_3$N$_4$/CoS$_x$, g-C$_3$N$_4$/MoS$_2$ and g-C$_3$N$_4$/Co$_{0.04}$Mo$_{0.96}$S$_2$ coated on ITO electrodes in a mixed solution of 10v/v% TEOA and Na$_2$SO$_4$ (0.1 mol/L) at pH 9 under visible light irradiation. The scan rate was 1 mV·s^{-1}.

In addition, the electrochemical H$_2$ evolution activities of g-C$_3$N$_4$, g-C$_3$N$_4$/CoS$_x$, g-C$_3$N$_4$/MoS$_2$ and g-C$_3$N$_4$/Co$_{0.04}$Mo$_{0.96}$S$_2$ nanohybrid deposited on ITO glass were also investigated using the linear sweep voltammetry (LSV) technique [35]. Fig.8-B shows the cathodic current of bare ITO electrode belonged to the reduction of water to H$_2$ was extremely low even at high applied potentials. The cathodic currents of ITO/g-C$_3$N$_4$, ITO/g-C$_3$N$_4$/CoS$_x$, ITO/g-C$_3$N$_4$/MoS$_2$ and ITO/g-C$_3$N$_4$/Co$_{0.04}$Mo$_{0.96}$S$_2$ electrode had a significant improvement beyond -0.4 V. And the highest current density was observed from ITO/g-C$_3$N$_4$/Co$_{0.04}$Mo$_{0.96}$S$_2$ electrode, which proved that g-C$_3$N$_4$/Co$_{0.04}$Mo$_{0.96}$S$_2$ was a remarkable co-catalyst which can efficiently catalyze the reduction of water to H$_2$. This result further testify cobalt doping in the g-C$_3$N$_4$/MoS$_2$ can accelerate the electrons transfer.

The speculation of mechanism for H_2 evolution
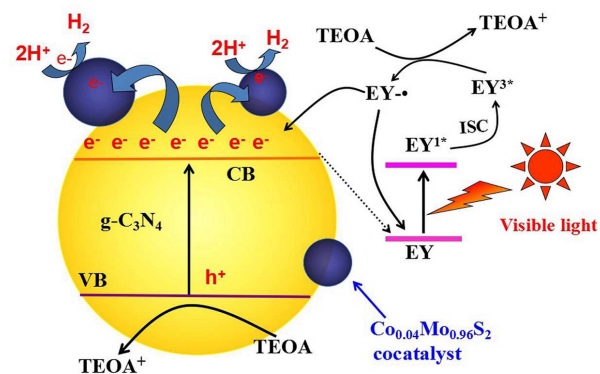
Scheme 1 The proposed photocatalytic mechanism for hydrogen evolution over EY-g-C_3N_4/$Co_{0.04}Mo_{0.96}S_2$ photocatalysts under visible light irradiation.

Based on the above results, the reaction process of photocatalysis H_2 evolution in EY-sensitized g-C_3N_4/$Co_{0.04}Mo_{0.96}S_2$ system can be explained in terms of the Scheme 1. The cobalt significantly enhanced the photocatalytic hydrogen evolution activity maybe be attribute to the synergistic effect of the g-C_3N_4/MoS_2 and the Co-Mo-S structures. The Co-promoter is associate with Mo atoms creation most sites formation of differnent exposed facets of Co-Mo which have different degrees of coordinative unsaturation. Coordinatively unsaturated sites along the edges of catalyst particles are believed to the provide the active sites, where the dye molecules can absorb and undergo further reactions [19]. Under visible light irradiation, the absorbed EY on the surface of g-C_3N_4 sheets and $Co_{0.04}Mo_{0.96}S_2$ absorbs light photons to form singlet excited state EY^{1*}, and subsequently produces the lowest-lying triplet excited state EY^{3*} via an efficient intersystem crossing . The EY^{3*} is reductively quenched by TEOA to produce $EY^{-}\bullet$ and oxidative donor ($TEOA^+$) [24]. These electrons of $EY^{-}\bullet$ species are transferred to the conduction band of g-C_3N_4 and then to the loaded $Co_{0.04}Mo_{0.96}S_2$ catalyst where the protons are reduced to form molecular H_2. Simultaneously, the reduced state dye species get back to the ground state, accomplishing complete water reduction reaction. In addition, the g-C_3N_4 can also be excited by absorbing photons of light having energy exceeding its band gap and then transfer electrons directly to the $Co_{0.04}Mo_{0.96}S_2$ to produce H_2; however, the activity of the g-C_3N_4 is remarkably inferior to the sensitized sample. It is therefore concluded that the EY-sensitized g-C_3N_4 is effective and superior to the g-C_3N_4 in terms of practical applications for which photocatalysts with good visible light harvesting capability.

Conclusions

In summary, a novel photocatalysts g-C_3N_4/$Co_{0.04}Mo_{0.96}S_2$ with different exposed facets of Co-Mo was employed as catalysts for the examination of facet-dependent catalytic activity toward photocatalytic hydrogen evolution from water with Eosin Y photosensitized as antenna molecule under visible light irradiation. The g-C_3N_4/MoS_2 incorporation of Co with different exposed facets of Co-Mo exhibit high activity. The promoter Co atoms associated with Mo displayed the synergistic effects and efficiently induced photo-generated charge carriers and electron transfer. A possible reaction mechanism of the g-C_3N_4/$Co_{0.04}Mo_{0.96}S_2$ was corroborated by photo-luminescence spectra, photo-electro-chemical characterizations and electro-chemical impedance spectra studies. This study discloses the facet-dependent effect of metal-metal cocatalyst on semiconductor photo-catalysts in photo-catalytic water reduction, and will give an insight into design and synthesis of high-efficient metal/semiconductor hybrid photocatalysts. Fluorescence studies shown that the charge separation and the electrons transfer were more efficient in the condition of the cobalt addition. The different exposed facets of Co-Mo-S can not only contribute to the more efficiently absorb Eosin dye but also beneficial to efficiently transfer electrons due to the peculiar electron delocalization characteristics of Co-Mo-S structures. Thus, the unusual catalytic activity arises from the synergetic effects between g-C_3N_4/MoS_2 and the Co-Mo-S structures and a good long-term stability for H_2 evolution was obtained over the dye-sensitized g-C_3N_4/$Co_{0.04}Mo_{0.96}S_2$ photocatalyst. Based on the above results, the Co might be a promising alternative non-metal cocatalyst for the design new type of catalysts in photocatalysis proton reduction.

Acknowledgements

Notes and references

1 Z.W. Zhao, Y. Sun, F. Dong. *Nanoscale*, 2015,**7**, 15-37.
2 Z.L. Jin, X.Q. Hao, S.X. Min, J. Xu, H.Yuan, *Mater. Sci.* 2014, **20**, 392-395.

3   C. Kong, S.X. Min, G.X. Lu. *Chem. Commun.* 2014, **50**, 5037-5039.

4   X. Wang, K. Maeda, A. Thomas, K. Takanabe, G. Xin, J.M. Carlsson, K. Domen, M. Antonietti, *Nat.Mater.* 2009, **8**,76-80.

5   J.S. Zhang, X.F. Chen , K.Takanabe, K.Maeda, K.Domen, J.D. Epping, X.Z. Fu, M. Antonietti, X.C. Wang. *Angew. Chem.Int. Ed.*, 2010,**49**, 441-444.

6   K. Maeda, Phys. *Chem. Chem. Phys.*, 2013, **15**, 10537–10548.

7   Y.J. Zhang, T. Mori, J.H. Ye, M. Antonietti. *J. Am. Chem. Soc.*, 2010,**132**,6294-6295.

8   J.D. Hong, X.Y. Xia,Y.S. Wang, R. Xu. *J. Mater. Chem.*, 2012, **22**, 15006-15012.

9   G.G. Zhang, M.W. Zhang, X.X. Ye, X.Q. Qiu, S. Lin, X.C. Wang. *Advanced Materials*, 2014, **26**,805–809.

10 C.C. Han, L. Ge, C.F. Chen, Y.J Li, X.L. Xiao,Y.N. Zhang, L.L. Guo. *Applied Catalysis B:Environmental*, 2014, **147**, 546-553.

11 Y.S. Jun, E.Z. Lee, X.C Wang, W.H. Hong, G.D. NStucky, A. Thomas. *Advanced Functional Materials,* 2013, **23**, 3661–3667.

12 Y. Wang, J.D. Hong, W. Zhang, R.Xu. *Catal. Sci. Technol.*, 2013,**3**, 1703-1711.

13 Y. Hou, A.B. Laursen, J. Zhang , G. Zhang, Y. Zhu, X. Wang, S. Dahl , I.b Chorkendorff. *Angew. Chem. Int. Ed.,* 2013, **52**, 3621-3625.

14 C.C Han, L. Ge, C.F. Chen, Y.J. Li, X.L. Xiao, Y. Zhang, L.L. Guo. *Appl. Catal. B: Environ.*, 2014, **147**, 546-553.

15 M.G. Walter, E.L.Warren, J.R. McKone, S.W.Boettcher, Q. Mi, E.A. Santori, et al. *Chem Rev.* 2010,**110**,6446-6473.

16 L. Ge, C.C Han, X.L. Xiao, L.L. Guo. *Int.J. Hydro.Energy.* 2013, **38**, 6960-6969.

17 L. Ge, C.C Han, X.L. Xiao, L.L. Guo. *Appl. Catal. B: Environ.*, 2013,**142**,414-422.

18 H. Topsøe, B.S. Clausen, R. Candia, C. Wivel, S. Mørup. *Journal of Catalysis*, 1981, **68**, 433-452.

19 S. L. Byskov, J.K. Nørskov, B.S. Clausen, H. Topsøe. *Catalysis Letters,* 2000,**64**, 95–99.

20 Y.G. Li, H.L. Wang, L.M. Xie, Y.Y. Liang, G.S. Hong, H.J. Dai. J. Am. Chem. Soc., 2011, **133**, 7296–7299.

21 X. Zong, H.J. Yan, G.P. Wu, G.J. Ma, F.Y. Wen, L. Wang, C.Li. *J. Am. Chem. Soc.*, 2008, **130**, 7176–7177.

22 M. Shen, Z.P. Yan, L. Yang, P.W. Du, J.Y. Zhang, B. Xiang. *Chem. Commun.*, 2014, **50**, 15447-15449.

23 H. Zhao, Y. Dong, P.P. Jiang, H.Y. Miao, G.L. Wang, J.J. Zhang. *J. Mater. Chem. A*, 2015, **3**,7375-7381.

24 X.Q. Hao, Z.L. Jin, F. Wang, J. Xu, S.X. Min, G.X. Lu, *Superlattices and Microstructures*. 2015,**82**, 599-611.

25 C. Kong, S.X. Min, G.X. Lu. *Int. J. Hydrogen Energy*, 2014, **39**, 4836–4844.

26 G.G. Zhang, S.H. Zang, X.C. Wang. *ACS Catal.* 2015,**5**, 941-947.

27 G.G. Zhang, S.H. Zang, X.C. Wang. *Small*, 2015, **9-10**, 1215-1221.

28 Y.Y. Liang, Y.G. Li, H.L. Wang, J.G. Zhou, J. Wang, T. Regier, H.J. Dai. *Nature Materials*, 2011,**10**,780–786.

29 A. Gasparotto, D. Barreca, D. Bekermann, E. Tondello et al. *J. Am. Chem. Soc.*, 2011, **133**, 19362–19365.

30 Z.H. Pu, Q. Liu, A. M. Asiri, A.Y. Obaid, X. Sun. *Chem. Mater.*, 2014, **26**, 4326–4329.

31 J.V. Lauritsen, J. Kibsgaard, G.H. Olesen, F. Besenbacher et.al. *Journal of Catalysis*, 2007, **249**, 220–233.

32 H. Topsøe. *Applied Catalysis A: General*, 2007, **322**, 3–8.

33 H. Topsøe, B.S. Clausen. *Applied Catalysis*, 1986, **25**, 273-293.

34 L. Ge, F. Zuo, J. Liu, Q. Ma, C. Wang, D.Z. Sun, L. Bartels, P.Y. Feng, *J. Phys. Chem. C*, 2012, **116**, 13708–13714.

35 S.X. Min, G.X. Lu. *J. Phys. Chem. C*, 2012, **116**, 25415–25424.

36 W. Zhang, J. Hong, J. Zheng, Z. Huang, J. Zhou, R. Xu. *J. Am. Chem. Soc.*, 2011, **133**, 20680-20683.

Modulating Photogenerated Electron Transfer with Selectively Exposed Co-Mo Facet on a Novel Amorphous g-C$_3$N$_4$/Co$_x$Mo$_{1-x}$S$_2$ Photocatalyst

Xuqiang Hao[a], Zhiliang Jin[a*], Shixiong Min[a], Gongxuan Lu[b]

[a]School of Chemistry and Chemical Engineering, Beifang University of Nationalities, Yinchuan 750021, P.R.China

[b]State Key Laboratory for Oxo Synthesis and Selective Oxidation, Lanzhou Institute of Chemical Physics, Chinese Academy of Science, Lanzhou 730000, P.R.China
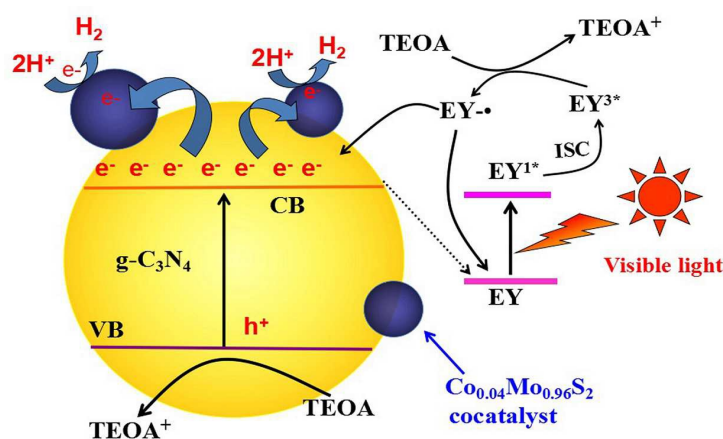
A novel photocatalysts g-C$_3$N$_4$/Co$_{0.04}$Mo$_{0.96}$S$_2$ with different exposed facets of Co-Mo was employed as catalysts for the examination of facet-dependent catalytic activity toward photocatalytic hydrogen evolution from water with Eosin Y photosensitized as antenna molecule under visible light irradiation. The promoter Co atoms associated with Mo displayed the synergistic effects and efficiently induced photo-generated charge carriers and electron transfer.